CHAPTER IV
RESULTS AND DISCUSSION

In this project, the catalysts were synthesized and investigated. There were calcined catalysts in powder form which were HY(P) and γ-Al_2O_3(P) and the extruded Pt/HY:pseudo boehmite (80:20), (60:40), (40:60), and (20:80) catalysts denoted as 80Pt/HY(E), 60Pt/HY(E), 40Pt/HY(E), and 20Pt/HY(E) respectively.

4.1 Characterization of Fresh Catalysts

4.1.1 Crystalline Phase Determination

The XRD diffraction patterns of 60Pt/HY(E) and HY(P) were collected by an XRD diffractometer. XRD analysis was determined a crystallization phases and the change in the structure of extruded HY zeolite due to the addition of pseudo boehmite binder. Figure 4.1 compares the XRD diffraction patterns of HY(P) and 60Pt/HY(E). The results showed that the diffraction pattern of 60Pt/HY(E) was similar to the calcined HY(P), indicating that the pseudo boehmite addition did not affect the HY zeolite structure. From Figure 4.2, XRD diffraction pattern present an amorphous phase of calcined pseudo boehmite (P) at 500 °C for 4 h. At higher temperatures, pseudo boehmite is transformed to γ-alumina but the pore size distribution remains unchanged up to 1,000 °C (Nogi *et al.*, 2012).

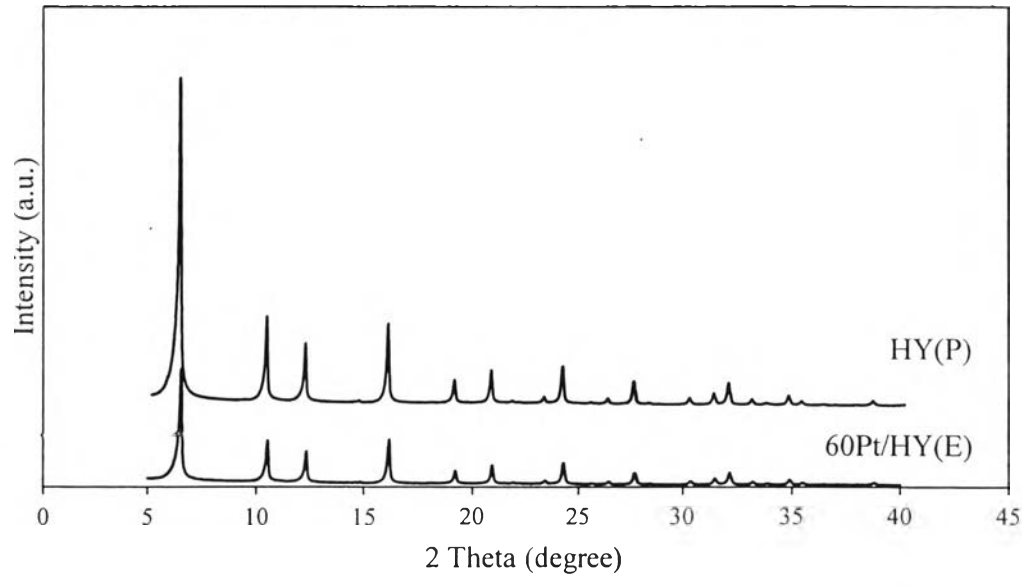

Figure 4.1 XRD patterns of 60Pt/HY(E) and HY (P).

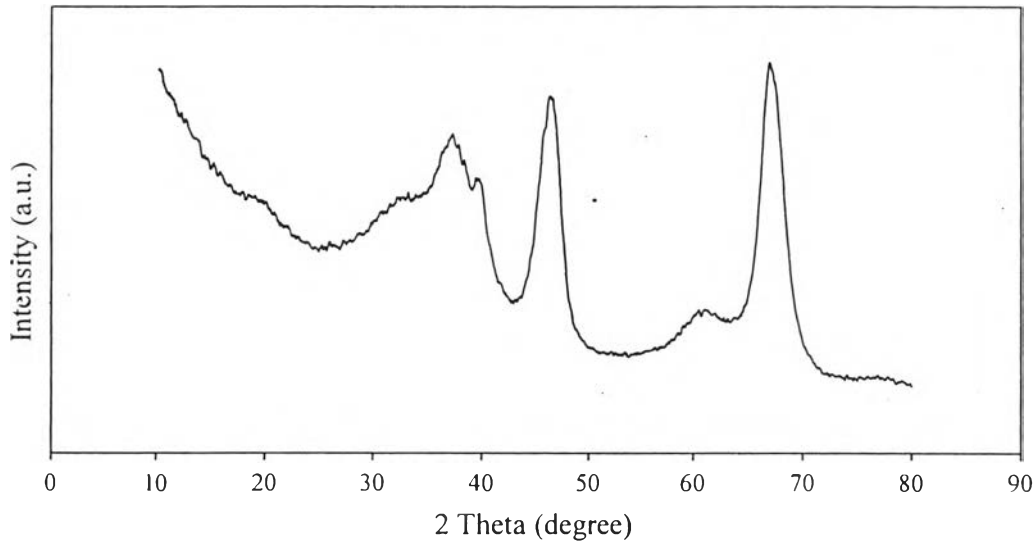

Figure 4.2 XRD patterns of calcined pseudo boehmite (P).

4.1.2 Brunauer-Emmett-Teller (BET)

The nitrogen adsorption isotherms were performed by BET surface area analyzer (Quantachrome/Autosorb-1). Specific surface area was calculated with the BET equation. Table 4.1 shows the surface area of extruded Pt/HY zeolite with

different percentages of pseudo boehmite binder. The result shows that the surface area of extruded Pt/HY was less than the Pt/HY because pseudo boehmite had low surface area. Therefore, when percentage of pseudo boehmite was increased, surface area of catalysts decreased. It can be determined that some pseudo boehmite species are embedded in the pore of HY zeolite, which would block the micropore's mouths of the zeolite and lead to a decline in surface area (Sheng. *et al.*, 2014).

Figure 4.3 shows the pore size distribition of extruded Pt/HY zeolite with different percentage of pseudo boehmite binder. The graph presents that the calcined HY zeolite had micropores with 0-20 Å and calcined pseudo boehmite had mesopores with 20-350 Å. By increasing the composition of pseudo boehmite, the fraction of mesoporous structure was increased.

Table 4.1 Physical characteristics of prepared catalysts

Catalyst	**BET Surface Area (m^2/g)**
Calcined HY zeolite(P)	633
Calcined pseudo boehmite(P)	242
80Pt/HY(E)	550
60Pt/HY(E)	486
40Pt/HY(E)	432
20Pt/HY(E)	340

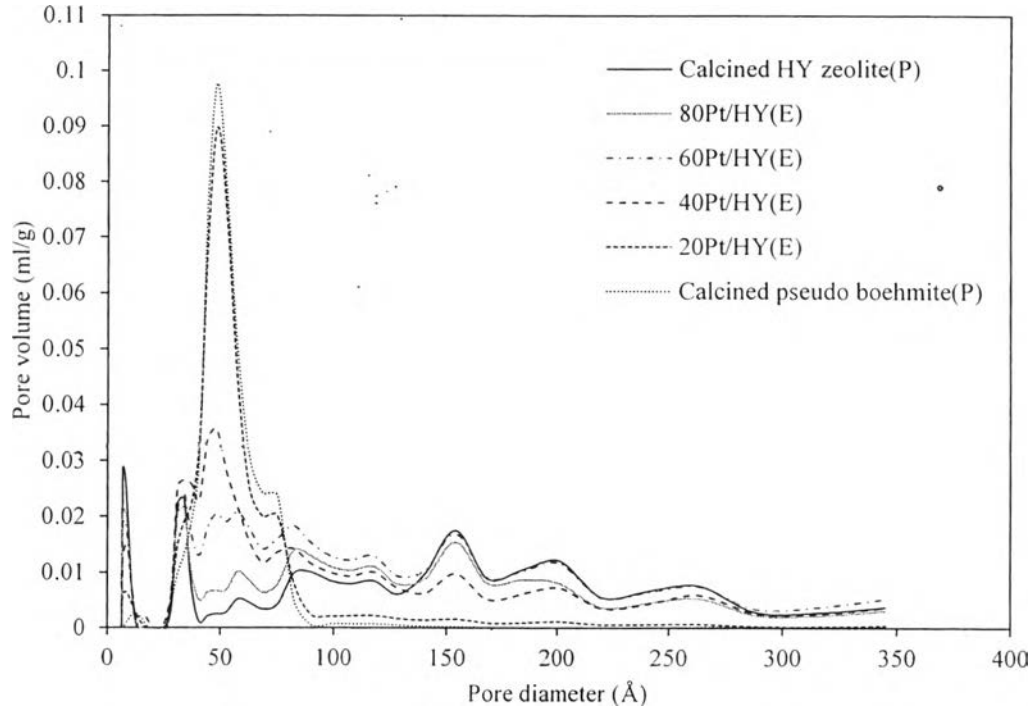

Figure 4.3 Pore size distribution of calcined HY zeolite(P), 80Pt/HY(E), 60Pt/HY(E), 40Pt/HY(E), 20Pt/HY(E), and calcined pseudo boehmite(P).

4.1.3 Temperature Programmed Desorption (TPD) of Isopropylamine

The temperature programmed desorption of isopropylamine that catalyzed the conversion of the isopropylamine into propylene and ammonia (Pereira *et al.*, 1992) is used to characterize the Brönsted acid sites of catalysts. TPD experiment was carried out using linear heating rate of 20 °C/min to study desorption and reaction of isopropylamine from HY zeolites supported catalysts. Figure 4.4 displays the m/z = 41 of propylene/isopropylene peak. All of catalysts exhibited Brönsted acid peak at approximately 380 °C. The acidity of the catalysts before and after exchanging with NH_4NO_3 and Pt is summarized in Table 4.2. It was found that the Brönsted acid site of the catalysts decreased with increasing the pseudo boehmite. The decrease in acidity could be due to the decreasing composition of HY zeolite. In addition, increasing the composition of pseudo boehmite, the peak of the Brönsted acid site was shifted to lower temperature. It can refer that adding of pseudo boehmite could influence on the strong acidity of extruded catalysts. After

exchanging the NH_4NO_3, the amount of Brönsted acid of catalysts were increased. Moreover, loading Pt on extruded catalyst slightly changed the acidity of catalysts.

Table 4.2 Acidity of the prepared catalysts from TPD of isopropylamine

Catalyst	Acidity of Catalysts (μmol/g)			
	Brönsted Acid			
	Catalyst	Extrudate	Extrudate $+NH_4NO_3$	Extrudate $+NH_4NO_3$+Pt
HY(P)	43.60			
Pt/HY(P)	33.5			
γ-Al_2O_4(P)	6.99			
Pt/γ-Al_2O_4(E)	6.20			
Pt/HY80(E)		32.32	35.44	20.33
Pt/HY60(E)		17.24	17.55	17.66
Pt/HY40(E)		16.04	17.16	17.15
Pt/HY20(E)		11.97	13.85	12.63

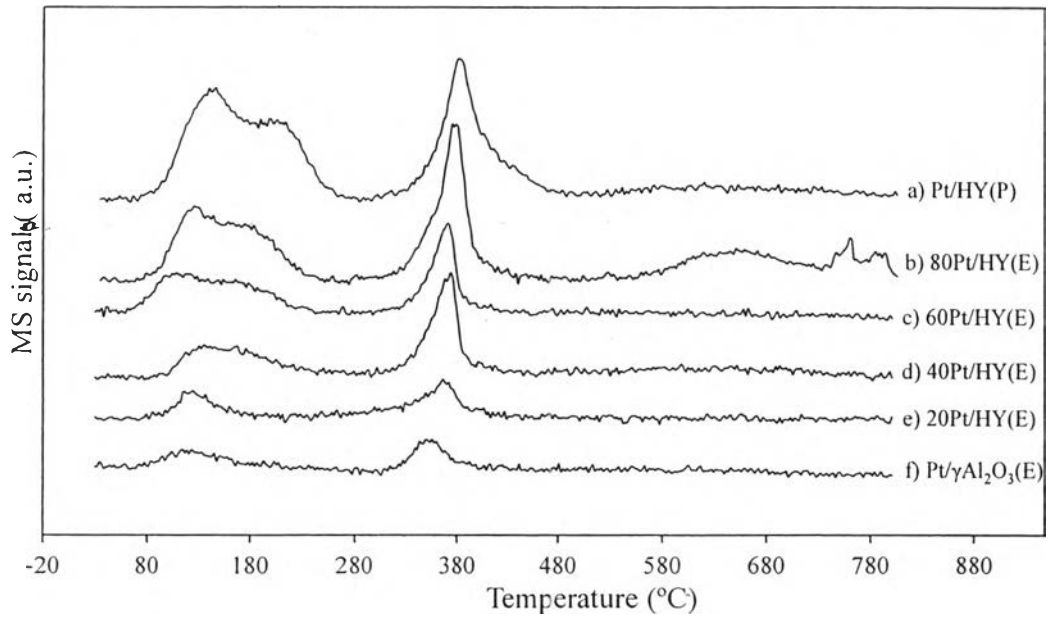

Figure 4.4 TPD of isopropylamine (IPA) of extruded HY zeolite with different percentage of (a) Pt/HY(P), (b) 80Pt/HY(E), (c) 60Pt/HY(E), (d) 40Pt/HY(E), (e) 20Pt/HY(E), and (f) Pt/γ-Al_2O_3(E) : m/z = 41, propylene/isopropylene.

4.1.4 Temperature Programmed Desorption (TPD) of Ammonia

Temperature programmed desorption of ammonia was performed the total acidity of Pt/HY(P), Pt/γ-Al_2O_3(E), and extruded catalysts with different percentages of pseudo boehmite binder. The m/z = 17 of ammonia peak was displayed in Figure 4.5. All of these catalysts exhibited physical adsorption and desorption peaks of ammonia at around 100 °C and 150-400 °C respectively. The total acidity of catalysts from TPD of ammonia compare with Brönsted acid from TPD of isopropylamine was shown in Table 4.3. The result shows that the total acidity of Pt/HY(P) was slightly higher than Brönsted acid indicating in low Lewis acid sites. For the extruded catalysts, the total acidity was obviously higher than the Brönsted acid. It can refer that adding with pseudo boehmite binder could generate the Lewis acid sites on extruded catalyst.

Table 4.3 Total acidity of the prepared catalysts from TPD of ammonia compare with Brönsted acid from TPD of isopropylamine

Catalyst	Total Acidity of Catalysts (μmol/g)	Brönsted Acid of Catalysts (μmol/g)
Pt/HY(P)	42.45	33.50
80Pt/HY(E)	64.51	20.33
60Pt/HY(E)	35.50	17.66
40Pt/HY(E)	34.61	17.15
20Pt/HY(E)	21.87	12.63
Pt/γ-Al_2O_3(E)	20.52	6.02

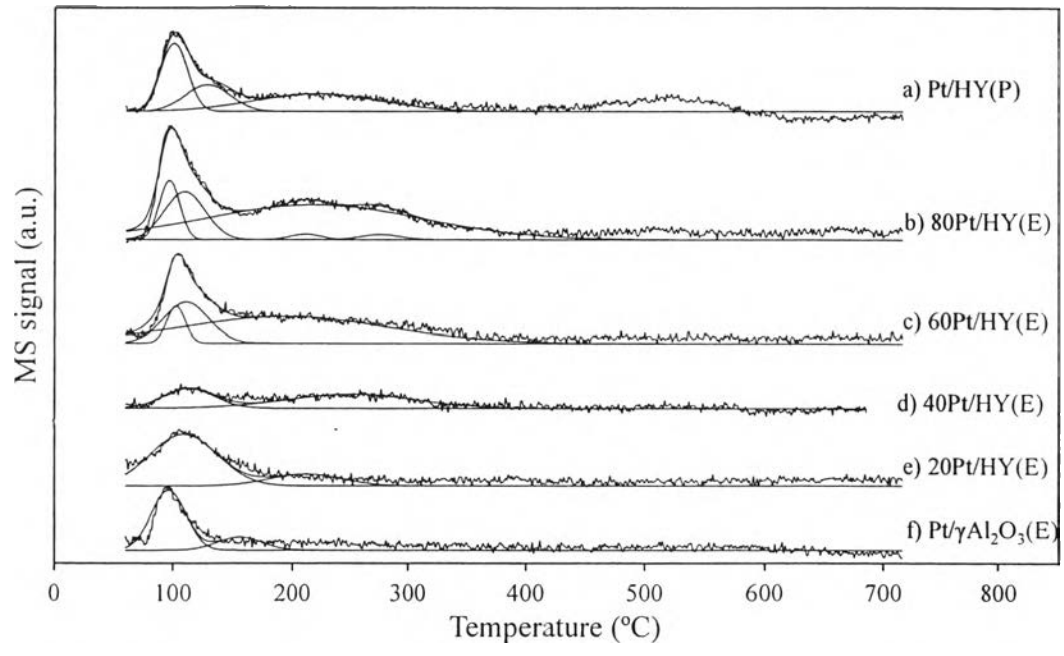

Figure 4.5 TPD of ammonia of extruded HY zeolite with different percentage of (a) Pt/HY(P), (b) 80Pt/HY(E), (c) 60Pt/HY(E), (d) 40Pt/HY(E), (e) 20Pt/HY(E), and (f) Pt/γ-Al_2O_3(E) : m/z = 17.

4.1.4 Temperature Programmed Reduction (TPR)

In order to investigate the reduction profile of the catalysts, temperature programmed reduction was used to evaluate the reduction temperature of the investigated catalysts. The TPR profiles of extruded Pt/HY catalysts with different percentages of pseudo boehmite binder after calcination at 350 °C are shown in Figure 4.6. The reduction profiles of all catalysts show the peak at around 100-300°C due to reduction of PtO_2 particles. The Pt^{4+} ions were formed under calcined conditions but the interaction was not strong (Ostgard *et al.*, 1992; Park *et al.*, 1986). For the catalyst with (a) Pt/HY(P) present the reduction peak at 420 °C. This peak was attributed to the reduction of Pt^{2+} located in super cages or sodalite units in the zeolite (Liu *et al.*, 1999). Considering (b) 80Pt/HY(E) and (c) 60Pt/HY(E), the reduction of Pt^{2+} were shifted to 500 °C. It can notice that the reduction of Pt/Al_2O_3 would occur (Phuong *et al.*, 2009). Next, the reduction profile

of d) 40Pt/HY(E), the peak near 420 °C remained the reduction of Pt^{2+} on zeolite due to high dispersion of Pt particle over HY zeolite. In addition, e) 20Pt/HY(E) and (f) Pt/γ-Al_2O_3(E) appear the small peaks near 600 °C which most likely associated with the reduction of Pt species in strong interaction with the γ-Al_2O_3 support (Liu, *et al.*, 2007).

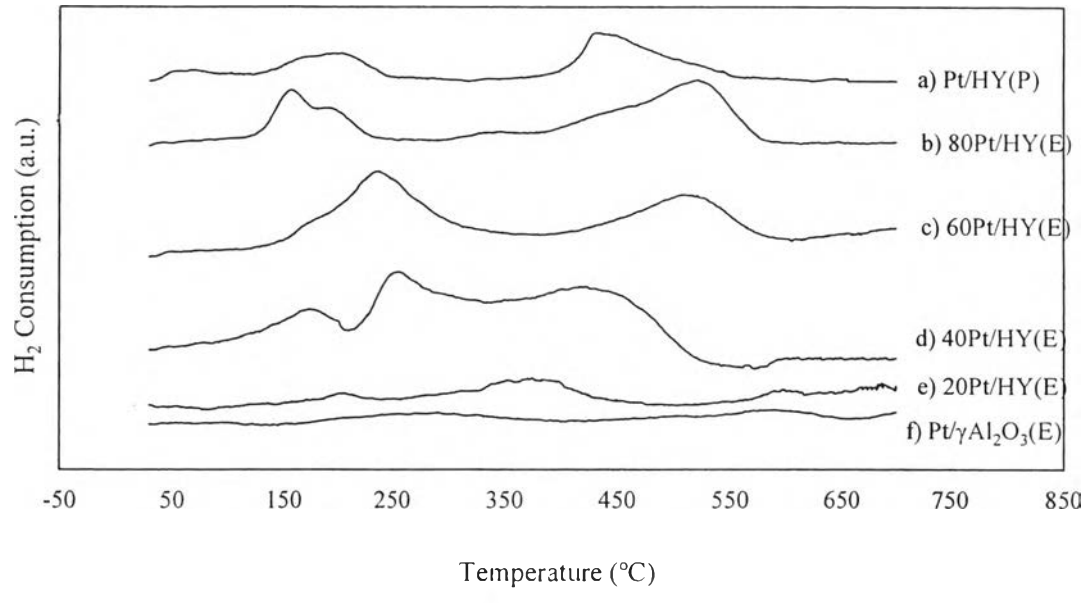

Figure 4.6 Temperature programmed reduction (TPR) profiles of (a) Pt/HY(P), (b) 80Pt/HY(E), (c) 60Pt/HY(E), (d) 40Pt/HY(E), (e) 20Pt/HY(E), and (f) Pt/γ-Al_2O_3(E).

4.2 Mechanical Characterization of Fresh Catalysts

4.2.1 Radial Crushing Strength

This research investigates the ability of pseudo boehmite binder which was added into the HY zeolite for shaping. Moreover, the effect of addition of glacial acetic acid with different percentages was also studied. Figure 4.7 exhibits the effect of varied vol% of glacial acetic acid for shaping parent pseudo boehmite. The strength of specimen increased when increasing the vol% of glacial acetic acid and started to decrease at 4 vol% of glacial acetic acid. Consequently, the addition glacial acetic acid was optimized concentration at 3 vol%. Figure 4.8 shows the strength of

extruded HY zeolite with different percentages of pseudo boehmite with 3 vol% of glacial acetic acid. The result shows that the more adding of pseudo boehmite content, the higher strength of catalysts.

Table 4.4 summarizes the mechanical properties of extrudate with different compositions of HY zeolite and pseudo boehmite ratios. All of prepared samples were calcined at 500 °C for 4 h. When the pseudo boehmite binder were added in HY zeolite for shaping, the mechanical properties of extrudate would be improved because of adhesive forces and cross-linking of terminal hydroxyl groups between neighboring binder particles (Sheng *et al.*, 2014).

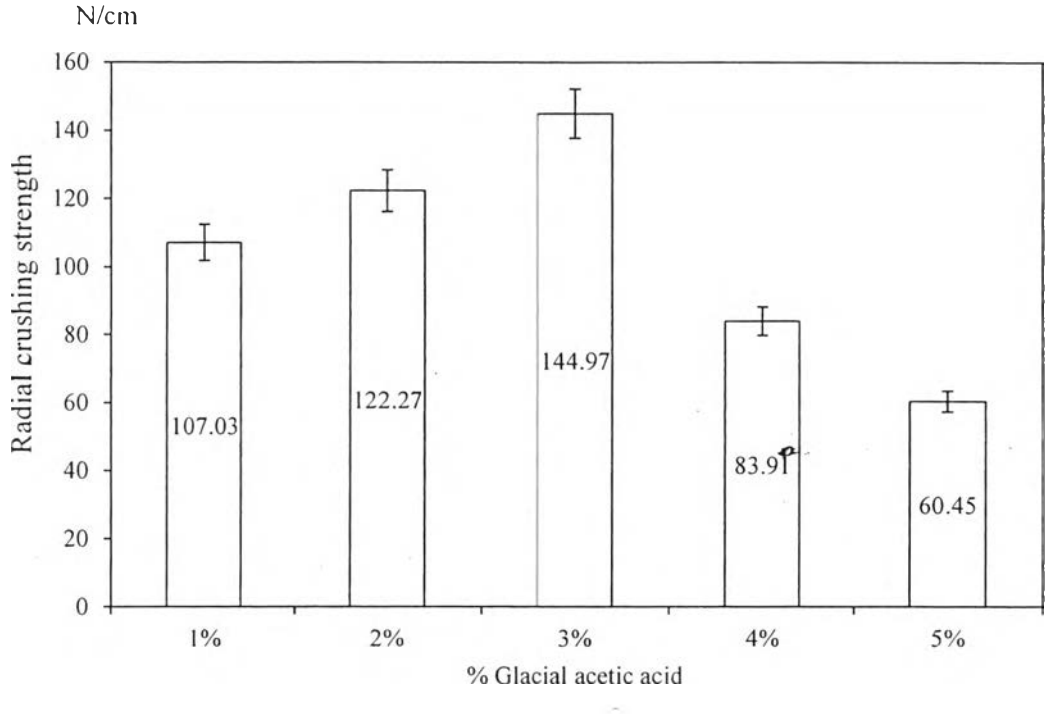

Figure 4.7 Radial crushing strength of extruded parent pseudo boehmite with varying percentages of glacial acetic acid.

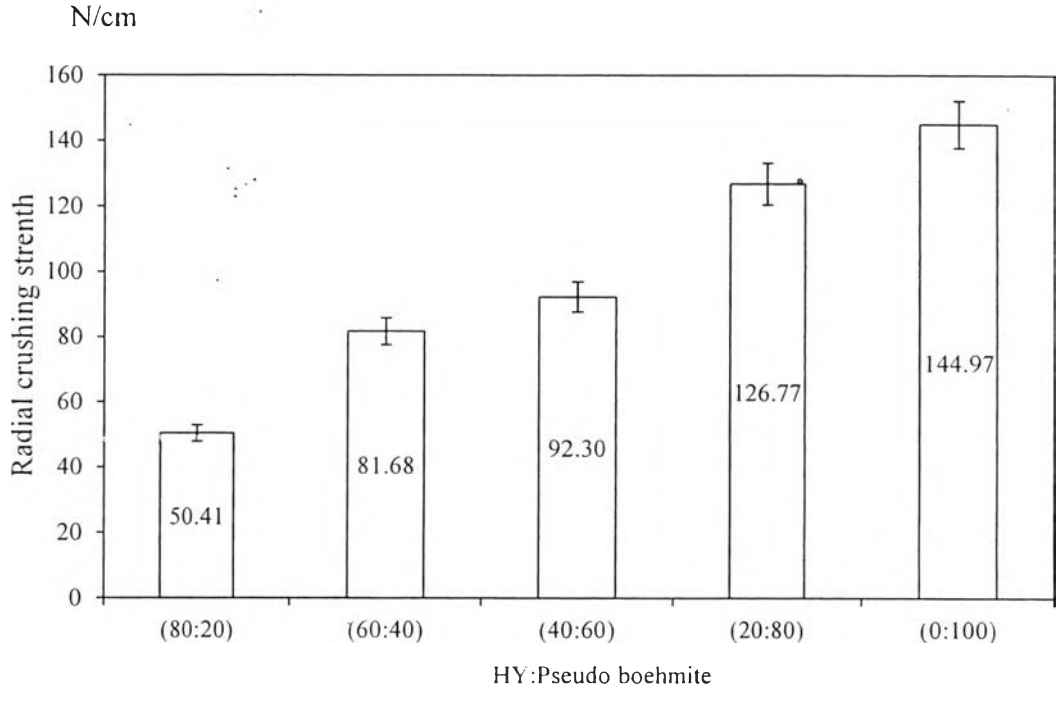

Figure 4.8 Radial crushing strength of extruded HY:pseudo boehmite with 3% glacial acetic acid.

Table 4.4 Mechanical properties of extrudate with different composition of HY zeolite and pseudo boehmite ratios

Characteristic	Unit	Extrudates (HY:Pseudo Boehmite) wt%				
		0:100	20:80	40:60	60:40	80:20
Diameter	mm	1.8	1.8	1.8	1.8	1.8
Length	mm	6.2	6.5	6.7	6.2	6.8
Bulk Density	g/cm^3			0.53		
Attrition Loss	wt%			0.96		
Radial Crushing Strength	N/cm	144.97	126.77	92.30	81.68	50.41

4.3 Feed and Standard Analysis

The chromatogram of various *n*-paraffin feedstock in the hydrogenated biodiesel range including pentadecane (*n*-C_{15}), hexadecane (*n*-C_{16}), heptadecane (*n*-C_{17}) and octadecane (*n*-C_{18}) analyzed by a GC/FID (Agilent 7890A) is shown in Figure 4.9. Besides peak of the *n*-paraffins, a little amount of *iso*-paraffins was also observed. Moreover, carbon disulfide was used as a solvent which appears on the chromatogram at 1.20 min.

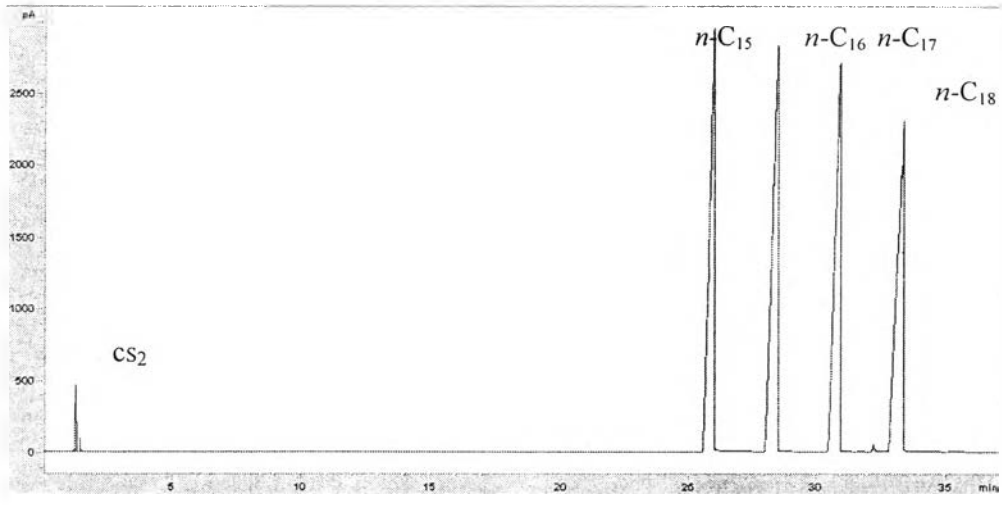

Figure 4.9 Chromatogram of various *n*-paraffin feedstock in the HBD range analyzed by a GC/FID.

In order to identify what each peak of liquid products, it is necessary to know the retention times for each product peak by using mixture of standard chemicals. The FID signal of standard chemicals is shown in Figure 4.10 and the retention times for each standard chemical is listed in Table 4.5.

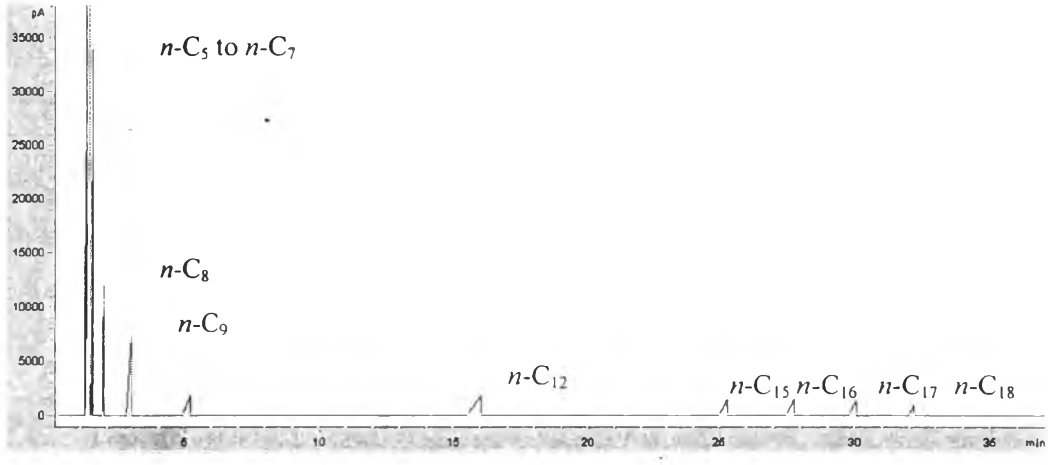

Figure 4.10 Chromatogram of standards chemicals including *n*-pentane (*n*-C_5), *n*-hexane (*n*-C_6), *n*-heptane (*n*-C_7), *n*-octane (*n*-C_8), *n*-nonane (*n*-C_9), *n*-decane(*n*-C_{10}), *n*-dodecane (*n*-C_{12}), *n*-pentadecane (*n*-C_{15}), *n*-hexadecane (*n*-C_{16}), *n*-heptadecane (*n*-C_{17}), *n*-octadecane (*n*-C_{18}) analyzed by a GC/FID.

For the reference standard of gas products, it was analyzed by a GC/FID (Shimadzu GC-17A) equipped with HP-Plot Al_2O_3 column. The FID signal of standard gas mixture is shown in Figure 4.11 and the retention times for each standard gas mixture are also listed in Table 4.5.

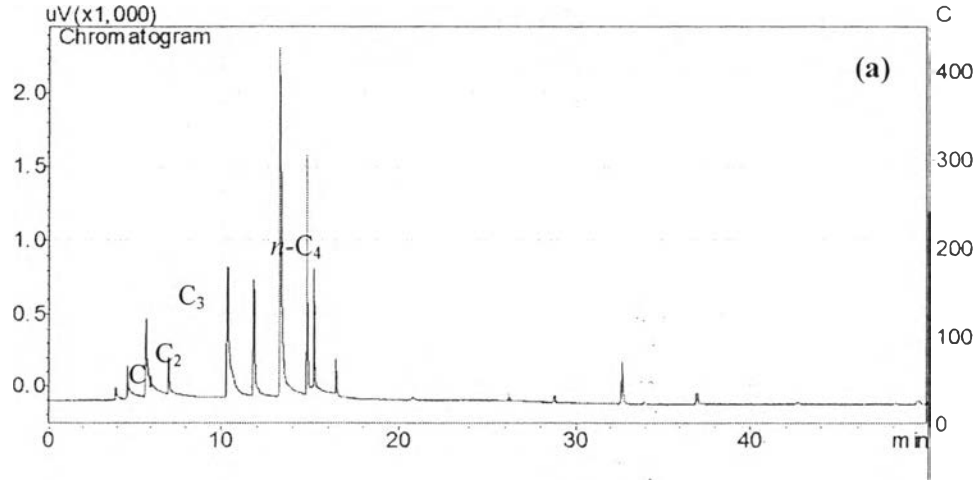

Figure 4.11 Chromatogram of the standard gases, (a) methane, ethane, propane and butane, (b) pentane, hexane, heptane, octane and nonane.

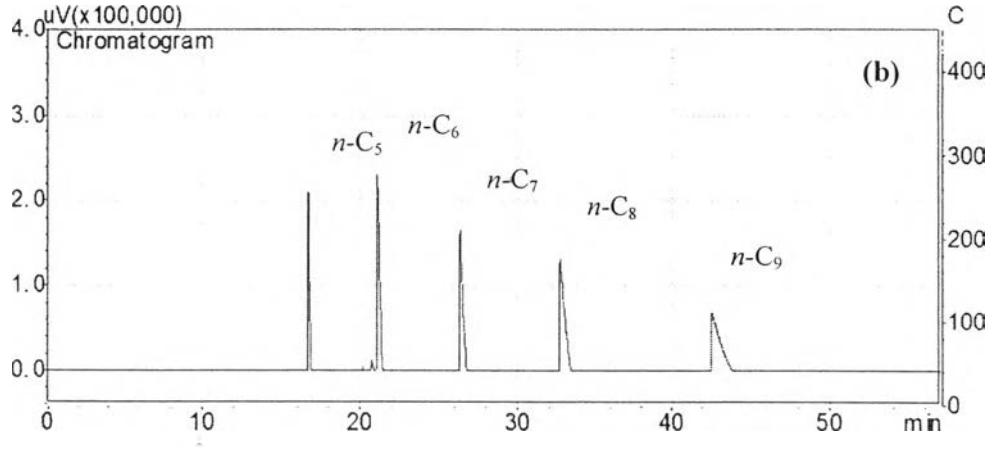

Figure 4.11 (Cont.) Chromatogram of the standard gases, (a) methane, ethane, propane and butane, (b) pentane, hexane, heptane, octane and nonane.

Table 4.5 Retention times of standard chemicals and standard gas mixture analyzed by a GC/FID (Agilent GC 7890A and Shimadzu GC-17A, respectively)

Standard Chemicals	Retention Times	Standard Gas Mixture	Retention Times
n-Pentane (*n*-C_5)	1.14	Methane (C_1)	3.92
n-Hexane (*n*-C_6)	1.26	Ethane (C_2)	4.56
n-Heptane (*n*-C_7)	1.44	Propane (C_3)	6.96
n-Octane (*n*-C_8)	1.89	*n*-Butane (*n*-C_4)	11.80
n-Nonane (*n*-C_9)	2.95	*n*-Pentane (*n*-C_5)	15.95
n-Decane (*n*-C_{10})	5.46	*n*-Hexane (*n*-C_6)	20.32
n-Undecane (*n*-C_{11})	11.19	*n*-Heptane (*n*-C_7)	26.13
n-Dodecane (*n*-C_{12})	16.26	*n*-Octane (*n*-C_8)	32.30
n-Tridecane (*n*-C_{13})	19.97	*n*-Nonane (*n*-C_9)	41.73
n-Tetradecane (*n*-C_{14})	22.96		
n-Pentadecane (*n*-C_{15})	25.95		
n-Hexadecane (*n*-C_{16})	28.39		
n-Heptadecane (*n*-C_{17})	30.76		
n-Octadecane (*n*-C_{18})	33.52		

For example, a chromatogram of liquid and gas products over Pt/HY (Si/Al ratio of 100) operated at operating conditions: 310 °C, 500 psig, LHSV of 1.0 h^{-1}, H_2/feed molar ratio of 30, and TOS of 6 h is shown in Figure 4.10 and 4.11, respectively. In Figure 4.12 (a),a chromatogram of liquid products, they are divided into three main parts which are gasoline fuel (C_5-C_9), jet fuel (C_{10}-C_{14}), and remaining feed or diesel fuel (C_{15}-C_{18}) at the retention times of 1.14-2.95 min, 5.46-22.96 min, and 25.95-33.52 min, respectively. And in Figure 4.12 (b), a chromatogram of gas products, consisting of light fuel (C_1-C_4) and gasoline fuel (C_5-C_8) at the retention times of 3.92-11.80 min and 15.95-32.30, respectively.

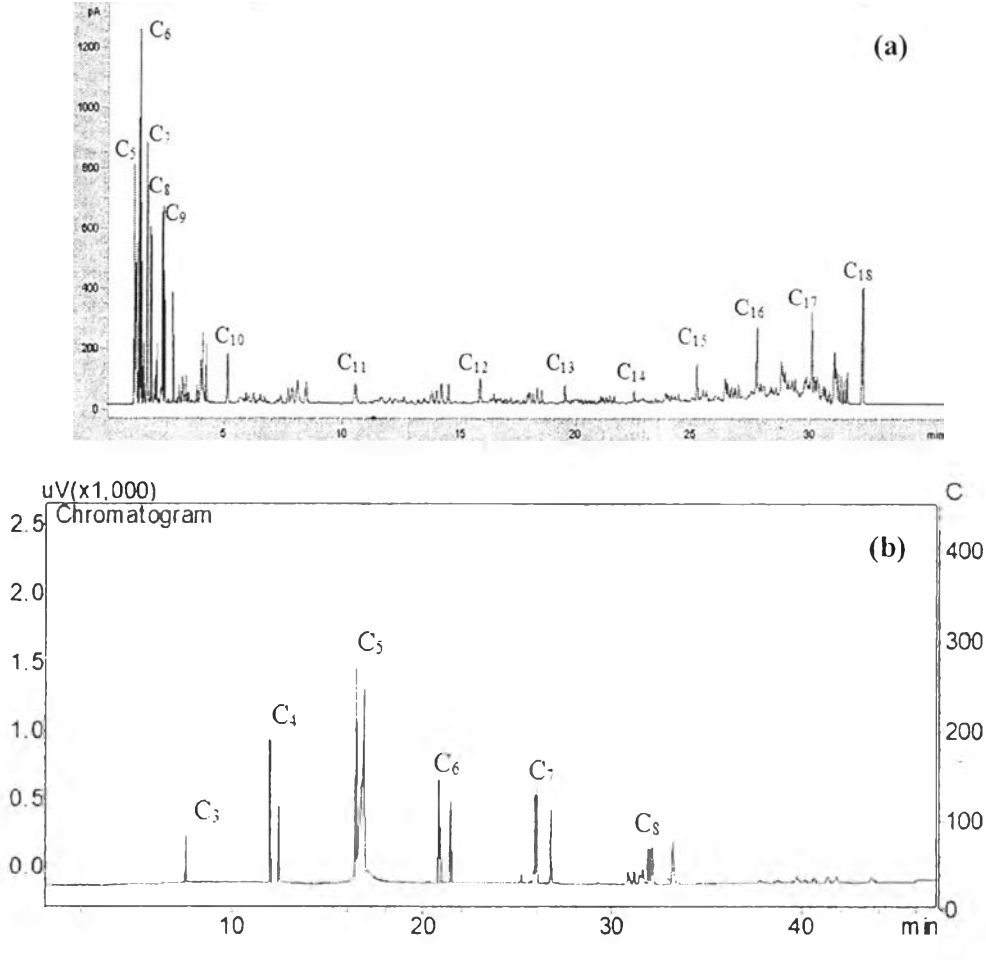

Figure 4.12 Typical chromatogram of (a) liquid products and (b) gas products over Pt/HY (Si/Al ratio of 100) operated at operating conditions: 310 °C, 500 psig, LHSV of 1.0 h^{-1}, H_2/feed molar ratio of 30, and TOS of 6 h.

Jet A-1 is the most commonly used commercial aviation fuel. It consists mainly of nonane (C9), decane (C10), undecane (C11), dodecane (C12), tridecane (C13), and tetradecane (C14) with high fraction isomerized paraffins which product distribution of jet A-1 is shown in Figure 4.13.

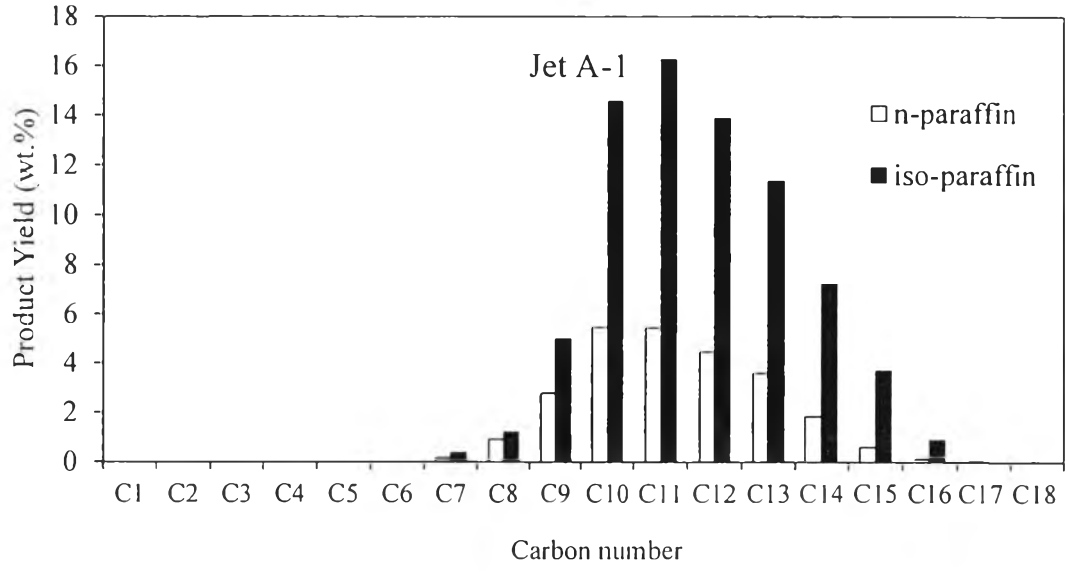

Figure 4.13 Product distribution of jet A-1 in term of yield.

4.4 Catalytic Activity Testing

For studying of the catalytic activity, conversion, product yield andproduct selectivity of extruded catalysts, HY zeolite was formulated by the addition of pseudo boehmite binder then the ion-exchanged techniques (IE) was used to load the Pt with 0.1 wt% on the extrudate. The reaction conditions for hydrocracking of hydrogenated biodiesel (HBD) were conducted at 310 °C, 500 psig, and H_2/feed molar ratio of 30.

4.4.1 Effect of LHSV

In this section, the result of catalytic activity testing of 60Pt/HY(E) was considered to optimize for producing in the range of jet fuel with high iso-paraffins compared to jet A-1. The operating parameter was varied by liquid hourly space velocity (LHSV), which indicates how many reactor volumes of feed can be

treated in a unit time. It is a dominant factor affecting FCC performance. To find the optimum reaction condition, the liquid hourly space velocity (LHSV) was varied from 1 to 3 h^{-1} to study this effect of reactions on product yields. The cracking reaction of hydrogenated biodiesel was performed at 310 °C, 500 psig, and H_2/feed molar ratio of 30. The product selectivity and conversion obtained over 60Pt/HY(E) with the different liquid hourly space velocity (LHSV) are given in Figure 4.14. From result indicates that the LHSV start from 1 h^{-1}, the conversion of product were closed to 100 % then dropped at around 2.5 h^{-1} because of the effect of contact time. At low LHSV, the feeds of hydrogenated biodiesel had enough time to react with catalysts in the reactor. Whereas, increasing the LHSV could provide the short contact time that the hydrocarbon were converted in continuous reactor decreasingly. For the selectivity of product obtained over 60Pt/HY(E) at LHSV 1 h^{-1}, the product selectivity consisted mainly of gasoline. When LHSV was increased, the selectivity of gasoline range was decreased. In the other hand, the selectivity of jet range tended to higher as increasing the LHSV due to the contact time among of catalysts and liquid hydrocarbon was brief. Therefore, the hydrogenated biodiesel was cracked into jet further.

Figure 4.15 exhibits the product yield over 60Pt/HY(E) with varied LHSV from 1 to 3 h^{-1}. When the LHSV were increased, the product yield of gasoline tended to low but the yield of jet tended to higher. At the LHSV 2.5 h^{-1}, product yield of jet was obtained highest around 19.46 %. However, increasing the LHSV influences the conversion of catalysts as well.

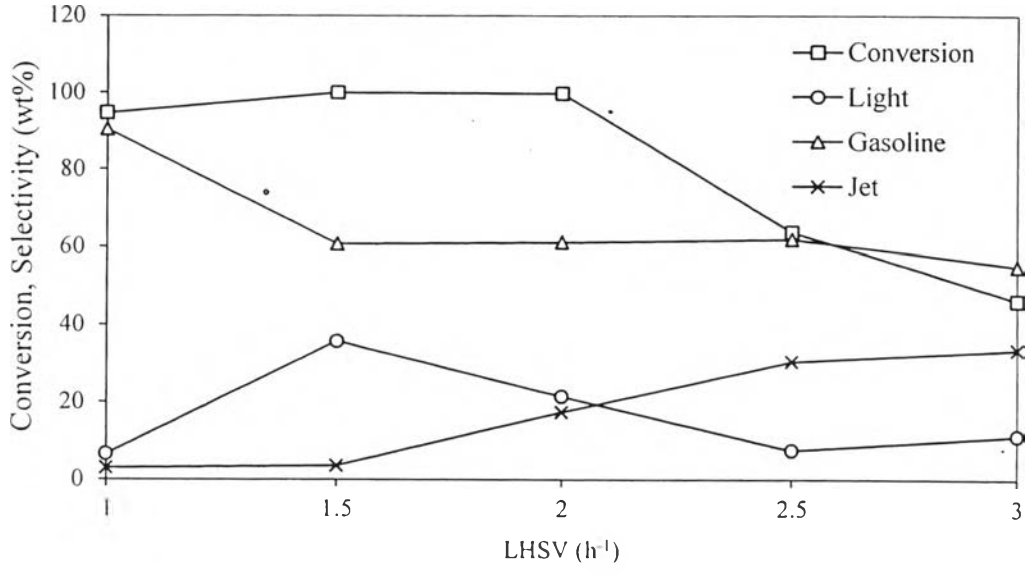

Figure 4.14 Product selectivity and conversion of hydrocracking of hydrogenated biodiesel (HBD) feedstock over 60Pt/HY(E) with varied LHSV from 1 to 3 h^{-1} operating condition: 310 °C, 500 psig, H_2/feed molar ratio of 30.

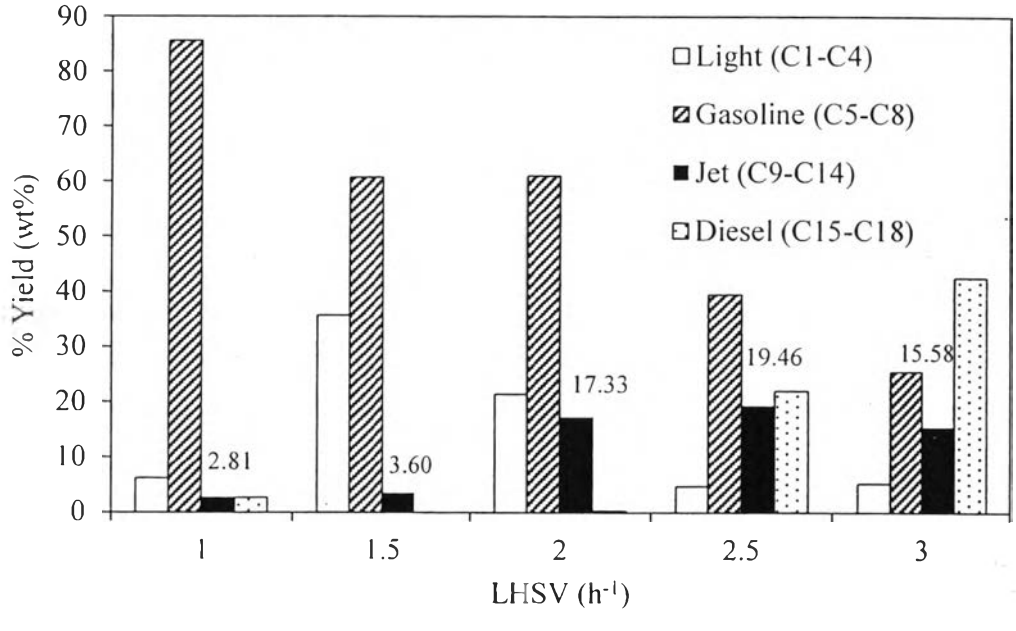

Figure 4.15 Product yield of hydrogenated biodiesel (HBD) feeds stock over 60Pt/HY(E) with varied LHSV from 1 to 3 h^{-1} operating condition: 310 °C, 500 psig, H_2/feed molar ratio of 30.

4.4.2 Effect of Catalyst Formulation

The HY zeolite catalyst was formulated by addition of the pseudo boehmite binder with 3 vol% of glacial acetic acid. The composition of pseudo boehmite was varied with 20 wt%, 40 wt%, 60 wt%, and 80 wt%. After that, the extruded catalyst was treated with NH_4NO_3 and loaded with 0.1 wt% of Pt. Figure 4.16 shows the distribution of liquid and gas product in term of product yield obtained over extruded Pt/HY zeolite with different percentages of pseudo boehmite binder. For more information, it was also shown in Figure 4.17 as the conclusive product distribution obtained over different extruded catalysts.

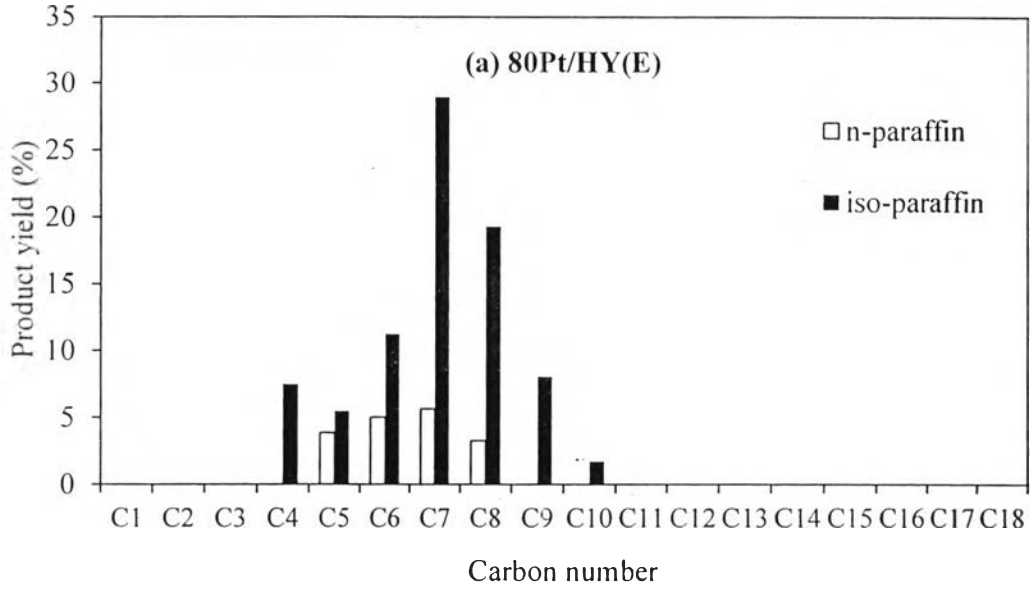

Figure 4.16 Product distribution in liquid and gas products in term of product yield obtained over (a) 80Pt/HY(E), (b) 60Pt/HY(E), (c) 40Pt/HY(E), (d) 20Pt/HY(E) (Reaction condition: 310 °C, 500 psig, and H_2/feed molar ratio of 30.

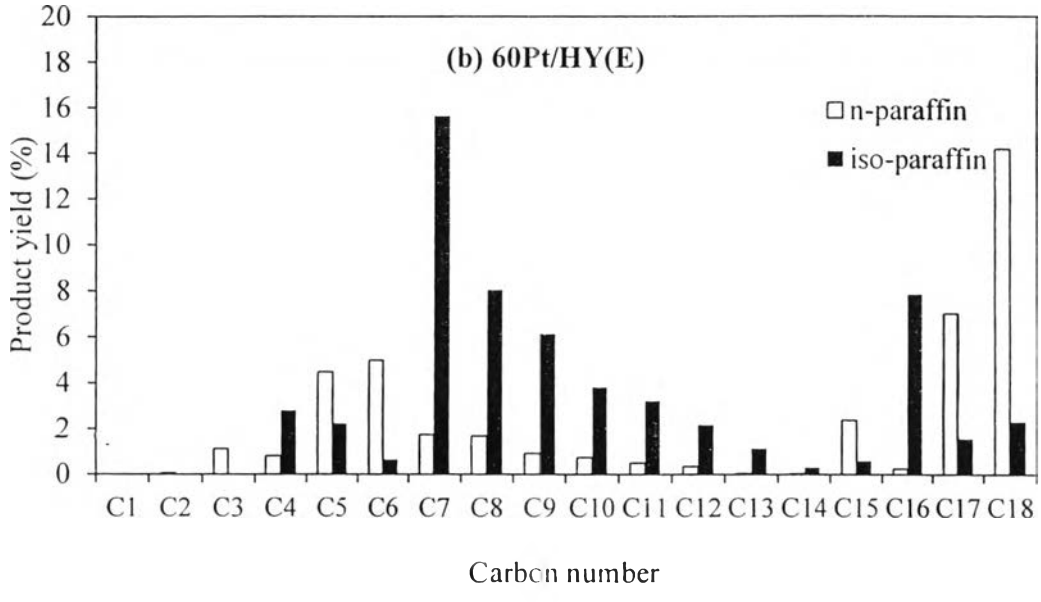

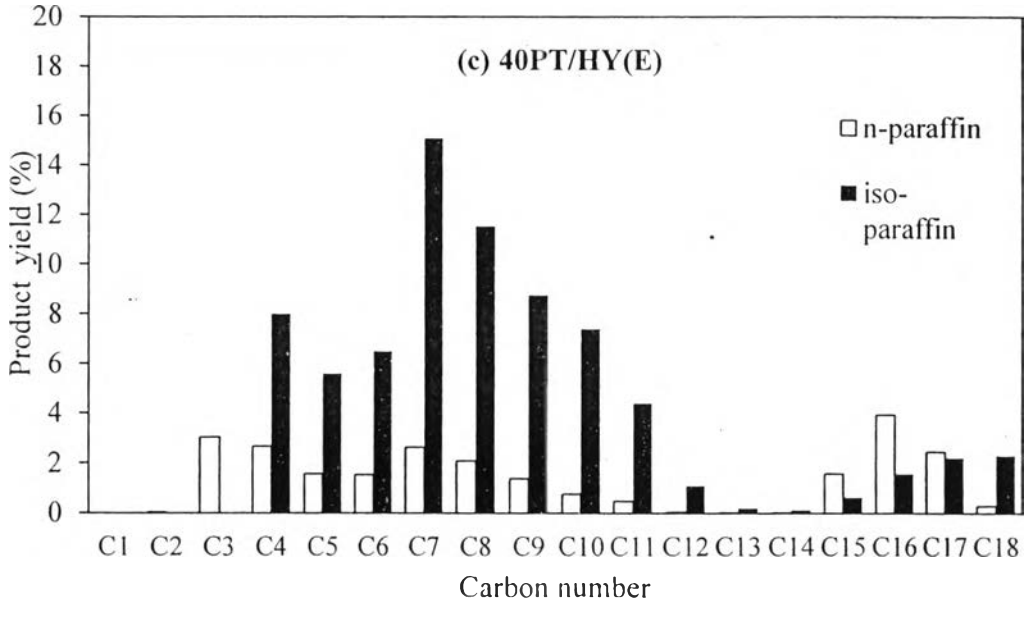

Figure 4.16 (Con't.) Product distribution in liquid and gas products in term of product yield obtained over (a) 80Pt/HY(E), (b) 60Pt/HY(E), (c) 40Pt/HY(E), (d) 20Pt/HY(E) (Reaction condition: 310 °C, 500 psig, and H_2/feed molar ratio of 30.

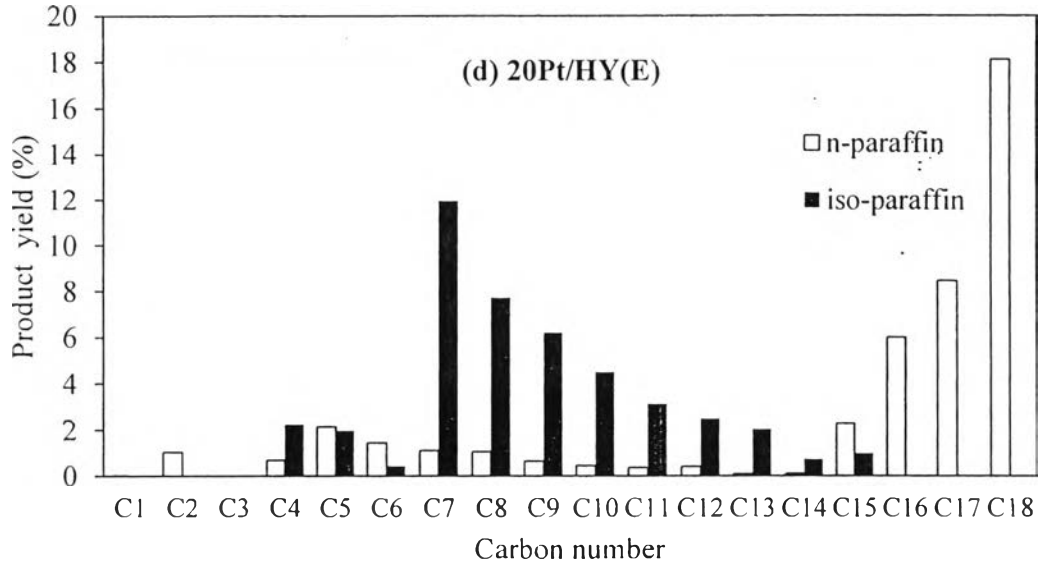

Figure 4.16 (Con't.) Product distribution in liquid and gas products in term of product yield obtained over (a) 80Pt/HY(E), (b) 60Pt/HY(E), (c) 40Pt/HY(E), (d) 20Pt/HY(E) (Reaction condition: 310 °C, 500 psig, and H_2/feed molar ratio of 30.

Figure 4.17 shows the comparison of products defined as light range (C_1-C_4), gasoline range (C_5-C_8), jet range (C_9-C_{14}) and remaining feed or diesel range (C_{15}-C_{18}) over catalysts. The result shows that the product obtained over Pt/HY(P) was high yield of jet fuel with 30.92 %. By contrast, the Pt/γ-Al_2O_3(E) did not convert the feedstock of hydrogenated biodiesel. Considering, all of the extruded catalysts, 80Pt/HY(E), 60Pt/HY(E), 40Pt/HY(E), and 20Pt/HY(E), gave the high yield of gasoline range compared with Pt/HY(P). From the TPD of ammonia data, the result exhibited that addition of pseudo boehmite binder could influence on increasing total amount of acidity of the extruded catalyst (Xiaobao *et al.*, 2013) which the Lewis acid sites were generated. There is evidence for the formation of Lewis acid site at extra-framework aluminum species and framework defects with occurring by silicon migration, formation of silanol groups or formation of hydroxyl groups at extra-framework aluminum (Weitkamp *et al.*, 2007). It induces the extruded catalysts with low hydrogenation-to-acidity ratios which can influence the rate of desorption of tertiary carbenium ion and selectivity of catalyst. The long-

chain molecules were not cracked in or near the center. Some of primary cracking reaction remains longer adsorbed at acid site and undergo secondary cracking. This results in higher yields in gasoline (Scherzer and Gruia 1996). In addition, transformation of pseudo boehmite binder into a γ form was sufficient both acid site and porosity. The large molecules of hydrocarbon were cracked into the molecular size which was capable to be further cracked by active site of zeolite into the gasoline or LPG range (Wolterman *et al.* 1980).

Comparing all of the extruded catalysts, the product obtained over 80Pt/HY(E) giving high yield of gasoline. When the Pt/HY was decreased to 60 wt%, the jet yield tended to higher until drop with decreasing the Pt/HY to 20 wt%. Moreover, decreasing the Pt/HY also decreased the yield of gasoline because the effect of total acidity of catalysts. In this research, 40Pt/HY(E) was the optimize ratio to obtain the highest yield of jet fuel with 24.73 %.

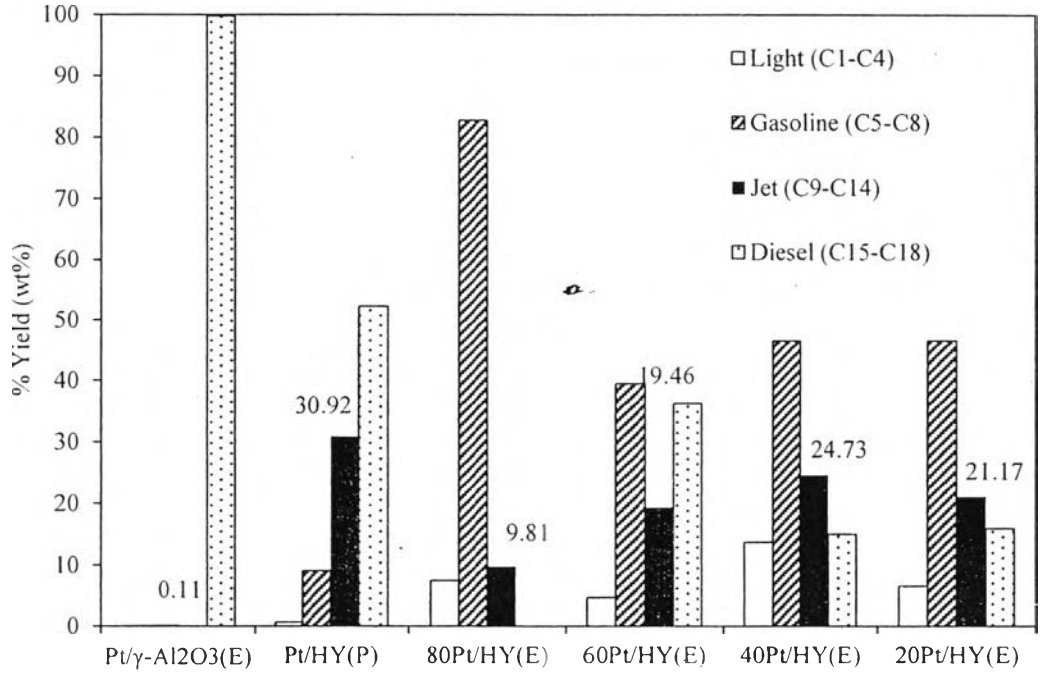

Figure 4.17 Product distribution obtained over different extruded catalysts compared with Pt/HY (Reaction condition: 310 °C, 500 psig, and H_2/feed molar ratio of 30).

Table 4.6 Liquid and gas product yield of different catalysts and jet A-1 yield (Reaction condition: 310 °C, 500 psig, and H_2/feed molar ratio of 30)

Catalysts		Jet A-1	HY	Pt/HY	Extruded Pt/HY:Pseudo boehmite			
					(80:20)	(60:40)	(40:60)	(20:80)
Yield of Gas Products (wt %)	C1	0	0	0.00	0	0	0	0.02
	C2	0	0	0.00	0	0.07	0.03	1.05
	C3	0	0	1.90	0	1.12	3.03	0.00
	C4	0	0	3.31	7.47	3.59	2.66	2.94
	C5	0	0	0.17	0	0.43	1.51	1.53
	C6	0	0	2.89	0	0.18	0.74	0.62
	C7	0	0	0.52	0	0.16	0.91	0.42
	C8	0	0	0.55	0	0.23	0.34	0.48
Yield of Liquid Products (wt %)	iso-C5	0	0	0.70	5.48	2.24	5.60	0.72
	n-C5	0	0	2.55	3.85	4.06	1.57	1.87
	iso-C6	0	0	1.83	11.24	0.66	6.49	0
	n-C6	0	0	0.95	5.00	4.80	1.53	1.26
	iso-C7	0.38	0.38	4.60	28.96	15.65	15.09	11.65
	n-C7	0.18	0.18	0.94	5.62	1.59	2.62	0.99
	iso-C8	1.21	1.21	4.20	19.30	8.06	11.54	7.54
	n-C8	0.92	0.92	0.78	3.27	1.44	2.08	0.79
	iso-C9	5.00	5.00	3.47	4.11	6.16	8.78	5.85
	n-C9	2.79	2.79	0.60	0.00	0.93	1.37	0.65
	iso-C10	14.57	14.57	2.86	1.75	3.82	7.41	4.51
	n-C10	5.46	5.46	0.47	0	0.74	0.76	0.46
	iso-C11	16.28	16.28	2.11	0	3.22	4.42	3.13
	n-C11	5.44	5.44	0.38	0	0.50	0.47	0.36
	iso-C12	13.90	13.90	1.44	0	2.17	1.10	2.49
	n-C12	4.46	4.46	0.29	0	0.35	0.05	0.40
	iso-C13	11.39	11.39	0.91	0	1.14	0.21	2.03
	n-C13	3.59	3.59	0.21	0	0.06	0.03	0.09
	iso-C14	7.22	7.22	0.21	0	0.32	0.12	0.75
	n-C14	1.83	1.83	0.17	0	0.03	0.02	0.10
	iso-C15	3.68	3.68	0.30	0	0.60	0.63	0.99
	n-C15	0.60	0.60	2.72	0	2.37	1.58	2.28
	iso-C16	0.91	0.91	1.35	0	7.88	1.58	2.28
	n-C16	0.14	0.14	7.97	0	0.25	3.94	6.03
	iso-C17	0.00	0.00	3.29	0	1.56	2.23	4.36
	n-C17	0.05	0.05	12.09	0	7.04	2.45	8.49
	iso-C18	0.00	0.00	3.23	0	2.31	2.32	4.41
	n-C18	0.00	0.00	30.01	0	14.22	0.30	18.11
Sum of Iso-paraffins (wt %)		74.53	5.49	68.69	68.53	54.95	69.02	57.32
Sum of N-paraffins (wt %)		25.47	94.51	31.31	31.47	45.05	30.98	42.68

Table 4.6 presents the liquid and gas product yields obtained over the different catalysts compared to Jet A-1. The results indicate that products consist mainly of isomerized paraffins obtained over Pt/HY(P), 80Pt/HY(E), 60Pt/HY(E), 40Pt/HY(E), and 20Pt/HY(E) catalysts. The extruded catalysts gave higher isomerized paraffins as a result of hydrocracking and hydrogenation over Pt/HY zeolite.

4.4.3 Effect of Different Acid Solutions

As resulted in catalytic activity testing, the 40Pt/HY(P) catalyst was the optimum for producing in the range of jet fuel with high iso-paraffins. In this section, the 3 vol% of nitric acid solution was used for formulation the HY catalyst to study this effect of reactions on product yields. The 3 vol% nitric acid solution was added to the mixture of HY zeolite and pseudo boehmite followed by the same method with using acetic acid for formulation. After that, the extrudate was loaded with Pt by ion-exchange method without treatment with ammonium nitrate.

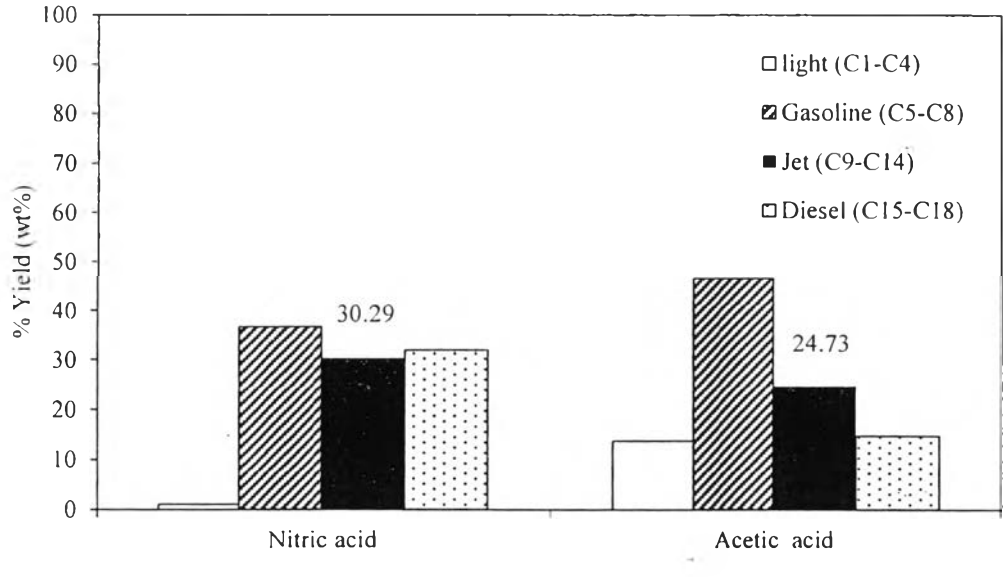

Figure 4.18 Product distribution obtained over 40Pt/HY(E) catalysts with different acid solution (Reaction condition: 310 °C, 500 psig, and H_2/feed molar ratio of 30).

The result in Figure 4.18 shows that the product yield of jet fuel obtained over 40Pt/HY(E) formulated by nitric acid solution with 30.29 wt%. It was higher yield of jet fuel than the 40Pt/HY(E) formulated by glacial acetic acid solution. For the mechanical properties, Figure 4.19 shows that the extrudate formulated with nitric acid have higher strength than other formulated with glacial acetic acid. Moreover, the 40Pt/HY(E) formulated by nitric acid solution could be converted the feedstock of hydrogenated biodiesel without treatment with ammonium nitrate. In the other hand, the 40Pt/HY(E) formulated by acetic acid solution could not convert the hydrogenated biodiesel if not treatment with ammonium nitrate. Nevertheless, the reason of this view was inscrutable to describe.

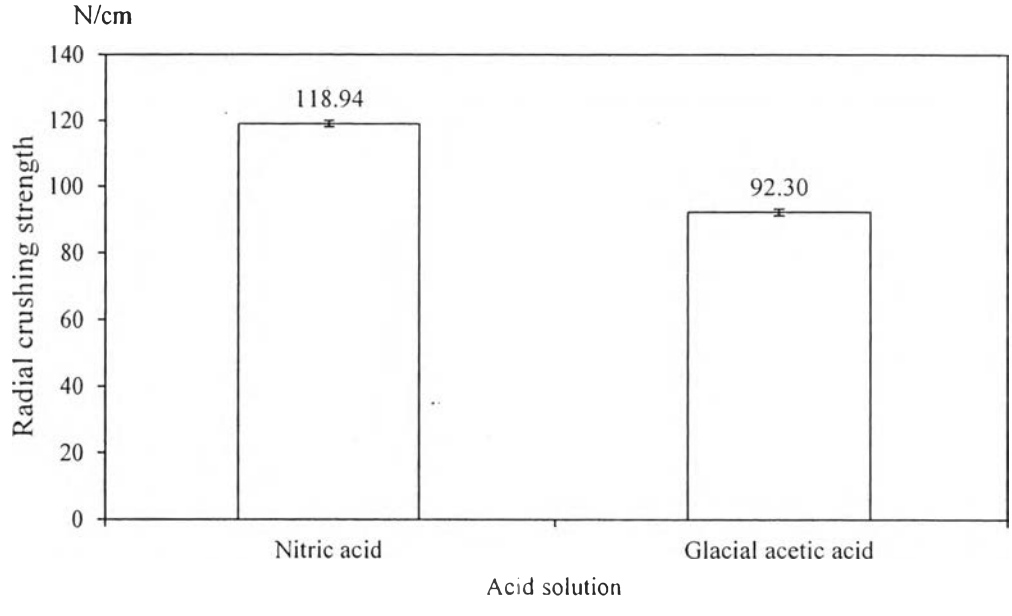

Figure 4.19 Radial crushing strength of extruded catalysts with different acid solutions.

Table 4.7 shows the surface area of 40Pt/HY(E) catalysts with different acid solution. The result shows that the surface area of 40Pt/HY(E) formulated by glacial acetic acid was less than the 40Pt/HY(E) formulated by nitric acid.

Table 4.7 Physical characteristics of 40Pt/HY(E) catalysts with different acid solution

Catalyst	**BET Surface Area (m^2/g)**
40Pt/HY(E) formulated by glacial acetic acid	432
40Pt/HY(E) formulated by nitric acid	450

Table 4.8 The total acidity from TPD of ammonia and Brönsted acid from TPD of isopropylamine of 40Pt/HY(E) catalysts with different acid solution

Catalyst	Total Acidity of Catalysts (μmol/g)	Brönsted Acid of Catalysts (μmol/g)
40Pt/HY(E) formulated by glacial acetic acid	64.51	20.33
40Pt/HY(E) formulated by nitric acid	82.45	33.50

The total acidity of catalysts from TPD of ammonia and Brönsted acid from TPD of isopropylamine of 40Pt/HY(E) catalysts with different acid

solution was shown in Table 4.8. The result shows that the total acidity and Brönsted acid of 40Pt/HY(E) formulated by nitric acid was slightly higher than the another formulated by glacial acetic acid. As acetic acid is a weak acid its dissociation power is weak (pKa=4.76) generating relatively small number of H^+ ions. Conversely, nitric is a strong acid which can completely dissociated in aqueous solution (pKa<1). Furthermore, the positive charge of catalyst could adsorb the counter ions of acetate ions which neutralized the proton on the catalyst (Van Garderen *et al.*, 2012). Hence, the extruded catalysts formulated by glacial acetic acid have to treatment with NH_4NO_3 to increase the proton on the extruded HY zeolite.